Comparative Study of an Electro Seismic Investigation of the BR52 and BR53 geothermal wells located on the Ohaaki Geothermal system near Taupo, NZ

M. Du Preez [1] ,J.R. McKendry [2] ,*N Knight* [3] ,*R Monckton* [4]

[1] *ATS, 11 Jac van Rhyn St, Universitas, Bloemfontein, 9301, South Africa*
[2] *ATS, 26 Emily St, Gisborne, 4010 , New Zealand*
[3] *ATS, 3 Lewis St, Gisborne 4010 , New Zealand*
[4] *ATS, 78 Walker Road Pt Chevalier, Auckland, 1022, New Zealand*

Key words: Geothermal, Electro seismic, Electro kinetic, Permeability, Electro seismic coupling coefficient, Ohaaki.

1 Introduction

1.1 Background

The first documented use of electro seismic methods occurred with Blau and Statham's (1936) patent application of a seismo electric geophysical investigation device. However, Frenkel (1944) was the first to publish a description on electric fields induced by the relative flow of fluid through a porous medium caused by a compressional seismic wave as it passed through the porous medium. Various authors continued on Frenkel's (1944) work between 1956 and 1994 resulting in the first seismo electrical model incorporating all of Maxwell's equations was developed by Pride (1994). The model described not only the co-seismic effects but also electro-seismic interface effects caused by streaming current imbalances within the seismic pressure wave as it passes between geological formations with different electro-seismic properties. Haartsen et al. (1998) then described these streaming currents in terms of permeability, porosity and salinity.

1.2 The electric double layer

Fitterman (1978) showed how unsatisfied chemical bonds at the surface of a mineral grain causes electrical charges. In the presence of electrolytic groundwater, these charges cause electric potentials between the charged surfaces and the water. Pride and Morgan (1991) show this electric potential causes an electric double layer, which is an effect of charge separation of the free ions within the water. The electric double layer consists of a, one ion layer thick, inner Stern layer, which is created by electrostatic forces drawing free ions within the water into the surface to satisfy the charge imbalances at the surface. These charge imbalances are however never fully balanced, causing an ordering effect of free ions within the water near the partially

charged surface to occur. This area of ordering is called the Gouy layer and constitutes the second layer of the electric double layer. The Stern and Gouy layers of the electric double layer are shown in figure 1. As the Stern layer is very thin, there is a strong drop off of potential difference across this layer. Boltzmann distributions can be used to describe the concentrations of ions in the Gouy layer, provided that the electrolytic content in the water is lower than 0.1 moles per liter. The thickness of the Gouy layer is called the Debye radius, donated by the letter d. The electric potential, φ, in the Gouy layer of diffused ions is described by the following equation:

$$\varphi(x) = \varphi_0 e^{-d/x}$$

Where:
d = inverse Debye radius
x = distance from the charged surface
φ_0=potential difference at the mineral surface

The slipping plane is the area where relative movement between the solid and water cause shearing between the outer diffused layer of ions and the inner strongly bound ions. This plain is not limited to the interface between the Stern and Gouy layers. Electric potential is produced by the shearing between the inner and outer ions of the Stern and Gouy Layers. This electric potential produced by the shearing effects is called the zeta (ζ) potential. The Zeta potential is one of the contributing variables used to describe the coupling of a seismic pressure wave to the resultant electric and magnetic fields produced due to the electro-kinetic effect.

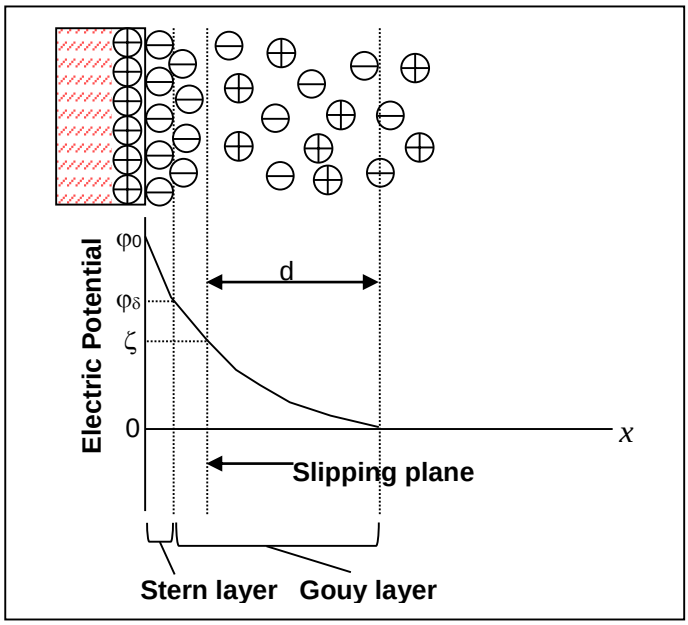

Figure 1 - Electric double layer

1.3 The electro seismic effect

The electro-seismic effect is observed when a seismic wave passes through a fluid saturated porous medium, causing relative movement between the solid medium and fluid as described by Du Preez (2005). This relative motion causes shearing between the ions in the fluid and the solid matrix, inducing a zeta potentials and streaming current within the medium. This effect is described by the following equation, Millar and Clarke (1997) :

$$\phi = -CP = -\left(\frac{\varepsilon\varepsilon_0\zeta}{\eta\sigma}\right)P$$

Where,
ϕ = electrical potential response or streaming potential
C = electro kinetic coefficient
P = applied pressure
$\varepsilon\varepsilon_0$ = permittivity of the pore space
ζ = zeta potential
η = fluid viscosity
σ = electrical conductivity

When the propagating seismic wave passes through a geological interface defined by geologies of differing electrical and mechanical properties, an imbalance in the streaming currents within the seismic wave is generated, resulting in an induced electric field. Thus, any porous, fluid saturated geological structure can be defined using electro-seismic methods. The basic equipment layout is shown in Figure 2. It consists of a grounded dipole antenna, made up of two stainless steel rods inserted 30cm into the ground, two meters apart. The seismic source consists of a 300kg drop weight located 30cm from the ground pin of the grounded dipole antenna. The 300kg weight is dropped from a height of 2.5m to induce a seismic energy pulse into the ground. The seismic pulse travels through the subsurface passing through fluid saturated porous rock formations where electro-seismic processes convert some of the seismic energy into electric field energy. The electric field instantaneously travels to the surface where the grounded dipole receives the electric fields as extremely weak, nano-volt level signals. These signals are amplified and digitally recorded as transient voltages by off the shelf analogy to digital converter equipment. As the Electro-seismic transient signals are in the seismic audio range, a sampling frequency of 44100Hz is used to acquire the transient voltages received. This allows the system to resolve geological structures to a maximum resolution of 10cm. This resolution is generally consistent with depth of investigation and geological structures can be defined from surface level to a maximum confirmed depth of 2400m, Du Preez and McKendry

(2010). However, the depth of investigation is limited only by the amount of seismic energy injected into the subsurface. In this study, a 300kg drop weight, dropped from 2.5m, combined with a data stacking approach, allowed for the definition of geological structures to a depth of 3000m. However, a larger weight dropped from a higher height would improve the depth of investigation.

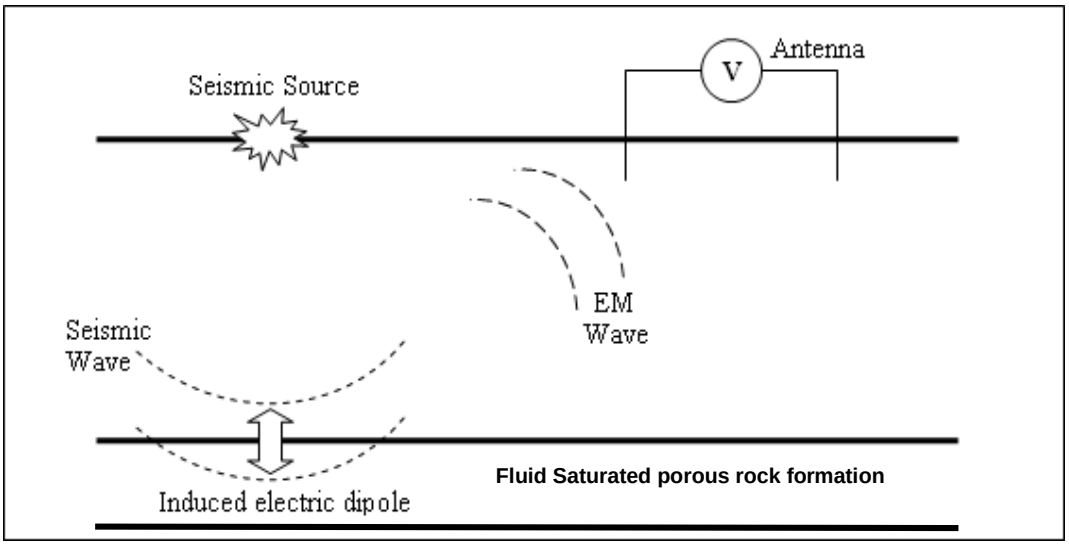

Figure 2 - Seismic wave crossing an interface generating an electromagnetic wave.

2 Site Description

The blind test site chosen for the study, provided by Contact Energy Ltd, is located within the Ohaaki West Geothermal System located near the town of Taupo. The Ohaaki Geothermal System is currently utilised for geothemal energy and the BR56, BR57 and BR58 geothermal well site is the central Western most drilled production capable wells in the field. It is ideally suited to a comparative study of the applicability of electro-seismic geophysical techniques to geothermal systems. This is due to the comprehensive well information available for the site. The survey site consist of fifteen survey points laid out in a line and analysed as a profiled line as shown in Figure 3. The site lies on a prepared well pad and has a number of manmade structures on it. The sounding points were located to the west of the structures to avoid any possible interference due to artificial noise sources. An inter-point spacing of 10m was used to gather high resolution data.

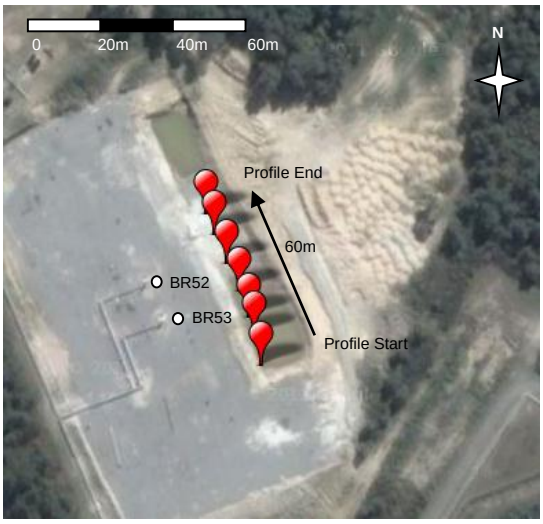

Figure 3 – Site description

Table 1 – BR52 Well information [21]

Well	Test 1
Location E Latitude	-38.517601°
Location S Longitude	176.305934°
Vertical Depth (m)	2092
Well Type	Deviated *Vertical to 450m then deviates to the east*

Table 2 – BR53 Well information [21]

Well	Test 2
Location E Latitude	-38.517735°
Location N Longitude	176.305982°
Vertical Depth (m)	1997
Well Type	Deviated *Vertical to* 1150m *then deviates to the west*

3 Site Geology and Lithology

The geology and lithology of the BR52 and BR53 bore site, provided after the electro seismic interpretation of the BR52 and BR53 wells as presented to Contact Energy, is shown in Tables 4 and 5. The main geothermal feeds lie in the Vitric-crystal breccias and welded crystal-lithic breccia/ignimbrite. The cooler aquifers lie in the Rhyolite lava formations. The geology is highly stratified under the BR52 and BR53 wells. However these two wells are highly localised and no information was provided beyond these wells. As such the geological interpretation for the site is not confirmed. The basement rock is estimated to be at a depth of 2100m. However this is not confirmed, directly under the test site, as the BR53 well was not drilled into the basement directly under the site. Table 4 and 5 are colour coded to indicate the corresponding

geologies between wells BR52 and BR53. This colour coding is also used to indicate formation logs on the ES analysis data shown in Figures 4.

Table4 BR53 Geological and Lithology Log

No	Depth (m)	Formation	Lithology
1	0	17	pumice alluvium
2	17	62	Siltstone/sandstone
3	62	472	Rhyolite lava
4	472	712	Tuffaceous rhyolite siltstone
5	712	742	Muddy siltstone
6	742	1092	Vitric-crystal breccias and laminated siltstone
7	1092	1387	welded crystal-lithic breccia/ignimbrite

Table5 BR52 well Geological and Lithology Log

No	Depth (m)	Formation	Lithology
1	0	17	pumice alluvium
2	17	62	Siltstone/sandstone
3	62	482	Rhyolite lava

Table 6 Site Hydrology

Depth	Description
175m	Cool Shallow aquifer 80°C
400m	Cool Shallow aquifer 130°C
750m	Geothermal Minor deep aquifer feed 220°C
950m	Geothermal Major deep aquifer feed 280°C

4 Site Hydrology

The site hydrology is summarised in table 6. There is one major feed at 950m depth. There are also two cooler aquifers at 175m and 400m depth. These known aquifer systems correlate well with the permeability results discussed in section 6.1.

5 Electro-Seismic Investigation

5.1 Hydraulic Conductivity Tomography

Figure 4A shows the electro seismic Hydraulic Conductivity tomography study results for the test site sounding profile. The positions and direction of this profile are indicated on Figure 3. The data is represented as hydraulic conductivity and expressed in meters per day. The values range from 0m/d to 2.6mm/d. Figure 4A also shows the relative position of the BR52 and BR53 wells when looking at the site from east to west as illustrated on Figure 3. This will allow the reader to visualise the aquifers with respect to these wells, as the discussion of results interpret the results from this point of view. The known aquifers are also shown on Figure 4A. The colour coded formation logs for wells BR52 and BR53 are also shown on the ES hydraulic conductivity tomography Plot in Figure 4A. These logs can be found in Table 4 and 5.

5.2 Electro Seismic Coupling Coefficient Tomography

Figure 4B shows the electro seismic coupling coefficient tomography data for the test profile. The ESCCT data is representative of the electrical characteristics that define the interaction between the pressure wave to electrical field conversion. The ESCCT data is expressed as a percentage of conversion. In geothermal systems, the electrical characteristics of the aquifer fluids dominate the conversion. Therefore in this study, the high response values are indicative of geothermal aquifer systems with high temperature and high fluid conductivity. Figure 4B also shows the relative position of the BR52 and BR53 wells when looking at the site from east to west as illustrated on Figure 3. This will allow the reader to visualise the aquifers with respect to these wells, as the discussion of results interpret the results from this point of view. The known aquifers are also shown on Figure 4B. The colour coded formation logs for wells BR52 and BR53 are also shown on the ESCCT Plot in Figure 4B. These logs can be found in Table 4 and 5.

5.3 Fracture Analysis

The fracture analysis tomography results shown in Figure 4C for the test profile show the inferred fracture zone depths. The electro seismic data is spectrally analysed and specific frequency patterns associated with fracturing are used to infer fracturing with depth. The results shown in Figure 4C are used to show secondary permeability within a primary permeability aquifer. These fractured zones are associated with higher fluid flow rates. Figure 4C also shows the relative position of the BR52 and BR53 wells when looking at the site from east to west as illustrated on Figure 3. This will allow the reader to visualise the aquifers with respect to these wells, as the discussion of results interpret the results from this point of view. The known aquifers are also shown on Figure 4C. The colour coded formation logs for wells BR52 and

BR53 are also shown on the ESFT Plot in Figure 4C. These logs can be found in Table 4 and 5.

5.4 Interface Tomography

Interface tomography shown for the test profile in Figure 4D, indicate the positions of interfaces between rocks or formations with different electrical resistivity. It makes use of the interface effects generated by electro seismic responses as the pressure wave passes through a rock resistive interface. This data can be used to determine if there are large geological shifts such as faults. Furthermore, the interface tomography results indicate positive and negative interface changes illustrated as red and blue respectively on Figure 4D. Interface response polarities indicate the type of fluids and rock involved in the generation ES response. Similar rock types generate similar polarity responses thus indicating stratification boundaries. This is very useful in determining which formations the geothermal responses occur in. Figure 4D also shows the relative position of the Test BR52 and BR53 wells when looking at the site from east to west as illustrated on Figure 3. This will allow the reader to visualise the aquifers with respect to these wells, as the discussion of results interpret the results from this point of view. The known aquifers are also shown on Figure 4D. The colour coded formation logs for wells BR52 and BR53 are also shown on the ESIT Plot in Figure 4D. These logs can be found in Table 4 and 5.

5.5 Electro-Seismic Fractures Associated with Geothermal Reserve Tomography

Fractured rock formations facilitate higher permeability and flow. However, this is only useful when the nature of the fracturing is understood. Fracturing often occurs at weak point in the subsurface rock formations. This weakness is often located at the interface between rock types of differing electrical and mechanical properties. Fractures occurring at these interfaces may play a significant role in resource flow if located within the relevant resource formation. Custom software allows the user to visualise fracturing associated with interface changes or inter formation fracturing. This data is shown in Figure 4H Figure 4H also shows the relative position of the BR52 and BR53 wells when looking at the site from east to west as illustrated on Figure 3. This will allow the reader to visualise the aquifers with respect to these wells, as the discussion of results interpret the results from this point of view. The known aquifers are also shown on Figure 4H. The colour coded formation logs for wells BR52 and BR53 are also shown on the ESFAGRT Plot in Figure 4H. These logs can be found in Table 4 and 5.

5.6 Electro-Seismic Change in Absolute Response Tomography

The electro seismic change in absolute gradient response is used to differentiate absolute electrical changes in rock formation properties. This method allows the user to discern formations of similar electrical characteristics and when used in conjunction with the electro seismic interface response tomography and ESCTRT, provides deeper insight into the geological and lithological information for subsurface formations. It is also used to support the delineation of subsurface faulting and intrusive formations not from an interface standpoint but rather from an absolute electrical standpoint. This data is shown in Figure 4E. Figure 4E also shows the relative position of the BR52 and BR53 wells when looking at the site from east to west as illustrated on Figure 3. This will allow the reader to visualise the aquifers with respect to these wells, as the discussion of results interpret the results from this point of view. The known aquifers are also shown on Figure 4E. The colour coded formation logs for wells BR52 and BR53 are also shown on the ESCTRT Plot in Figure 4E. These logs can be found in Table 4 and 5.

5.7 Electro-Seismic Change in Total Response Tomography

The electro seismic change in total gradient response is used to differentiate total electrical changes in rock formation properties. This method allows the user to discern formations of similar electrical characteristics and when used in conjunction with the electro seismic interface response tomography and ESCART, provides deeper insight into the geological and lithological information for subsurface formations. It is also used to support the delineation of subsurface faulting and intrusive formations not from an interface standpoint but rather from an total electrical standpoint. This data is shown in Figure 4F. Figure 4F also shows the relative position of the BR52 and BR53 wells when looking at the site from east to west as illustrated on Figure 3. This will allow the reader to visualise the aquifers with respect to these wells, as the discussion of results interpret the results from this point of view. The known aquifers are also shown on Figure 4F. The colour coded formation logs for wells BR52 and BR53 are also shown on the ESCTRT Plot in Figure 4F. These logs can be found in Table 4 and 5.

5.8 Electro-Seismic Resource Potential Tomography

The electro seismic resource potential tomography data shows the most likely position for resources. It combines all the most relevant electrical and hydrological properties of the formations under the site to determine the percentage probability of resource. This data is shown in Figure 4G. Figure 4G also shows the relative position of the BR52 and BR53 wells

when looking at the site from east to west as illustrated on Figure 3. This will allow the reader to visualise the aquifers with respect to these wells, as the discussion of results interpret the results from this point of view. The known aquifers are also shown on Figure 4G. The colour coded formation logs for wells BR52 and BR53 are also shown on the ESCTRT Plot in Figure 4G. These logs can be found in Table 4 and 5.

6 Discussion of results

6.1 Comparative study discussion

This discussion is with regards to the blind test data presented to Contact energy. No modifications or post presentation calibrations have been applied to the data, in order to provide an accurate indication of the ES methods performance on green field projects. The hydraulic conductivity results, shown in Figure 4A, indicate the high and low permeability areas under the site. The aquifer at 400m is high in primary permeability as indicated in Figure 4B. It is however not clearly visible on temperature estimation plot on figure 5. This may be due to the close temperature match between the best fit data and the actual aquifer temperature, thus indicating a very good temperature estimation but it does not help visually delineate the aquifer on Figure 5. The aquifer is also clearly visible in the ESCCT data, shown in Figure 4B, as a strong geothermal resource approximately 200m thick between 300m and 500m depth. This is due to a strong coupling effect caused by elevated temperature of 135°C that may have induced higher salt loads in the aquifer water. The ESCAGT data (Figure 4E) and ESCTGT (Figure 4F) indicate that the aquifer occurs at a strong electrical gradient change. This indicates change of geology or an interface between two geologies with large electrical property differences. This is supported by the well log data shown in Tables 4 and 5. The fracture tomography data, shown in Figure 4C, does not show any fracturing in the depth range of the aquifer, indicating that the aquifer does not have high secondary permeability. As such the aquifer has a low to medium flow rate. The resource probability data, shown in Figure 4G, shows that there is a high probability of geothermal resource at 400m depth. The aquifer at 950m is high in primary permeability as indicated in Figure 4B. It is clearly visible on temperature estimation plot on figure 5. The aquifer is also clearly visible in the ESCCT data, shown in Figure 4B, as a strong geothermal resource approximately 100m thick between 900m and 1000m depth. This is due to a strong coupling effect caused by elevated temperature of 280°C that may have induced higher salt loads in the aquifer water. The ESCAGT data (Figure 4E) and ESCTGT (Figure 4F) indicate that the aquifer occurs at a strong electrical gradient change.

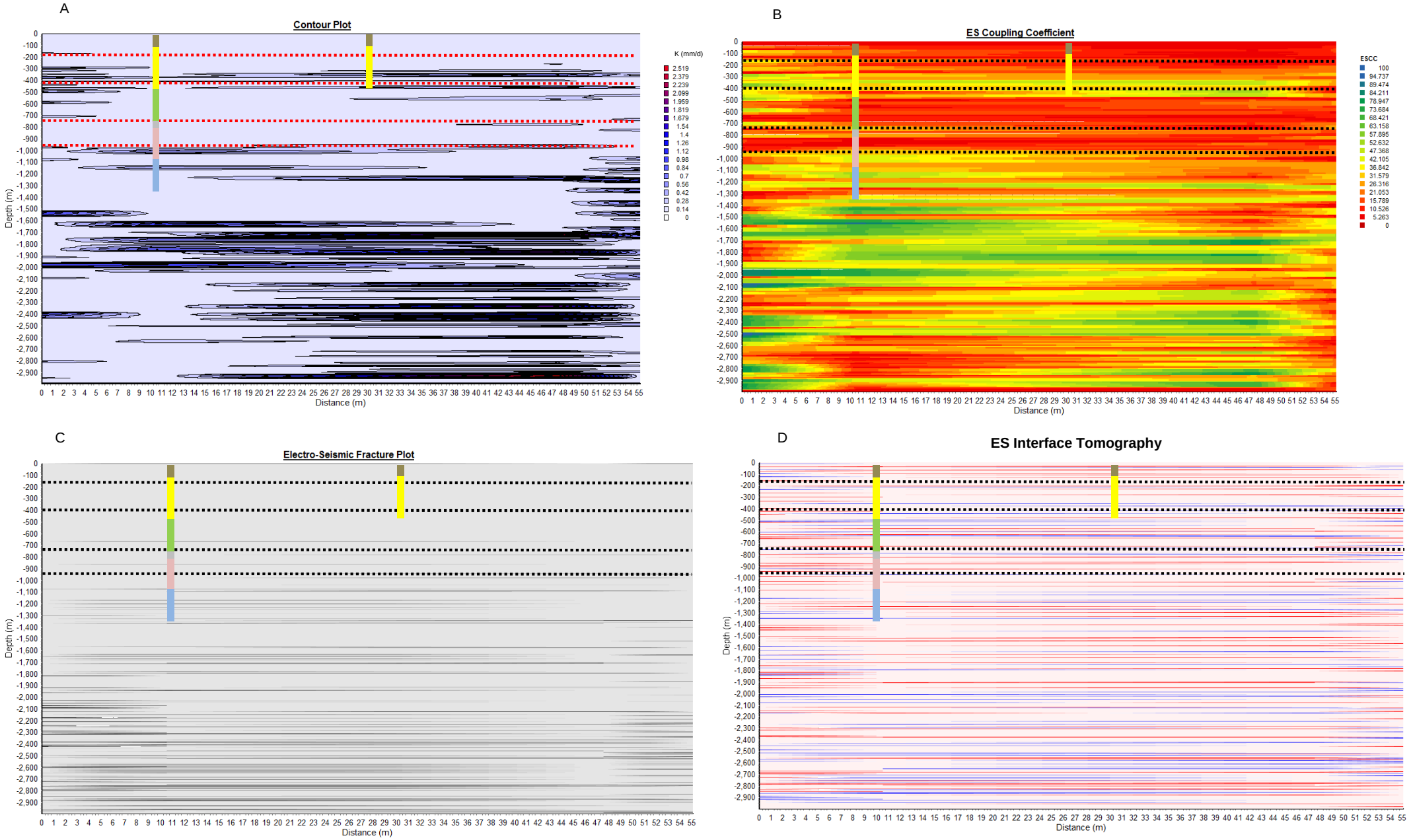

Figure 4 – Electro Seismic Data Analysis

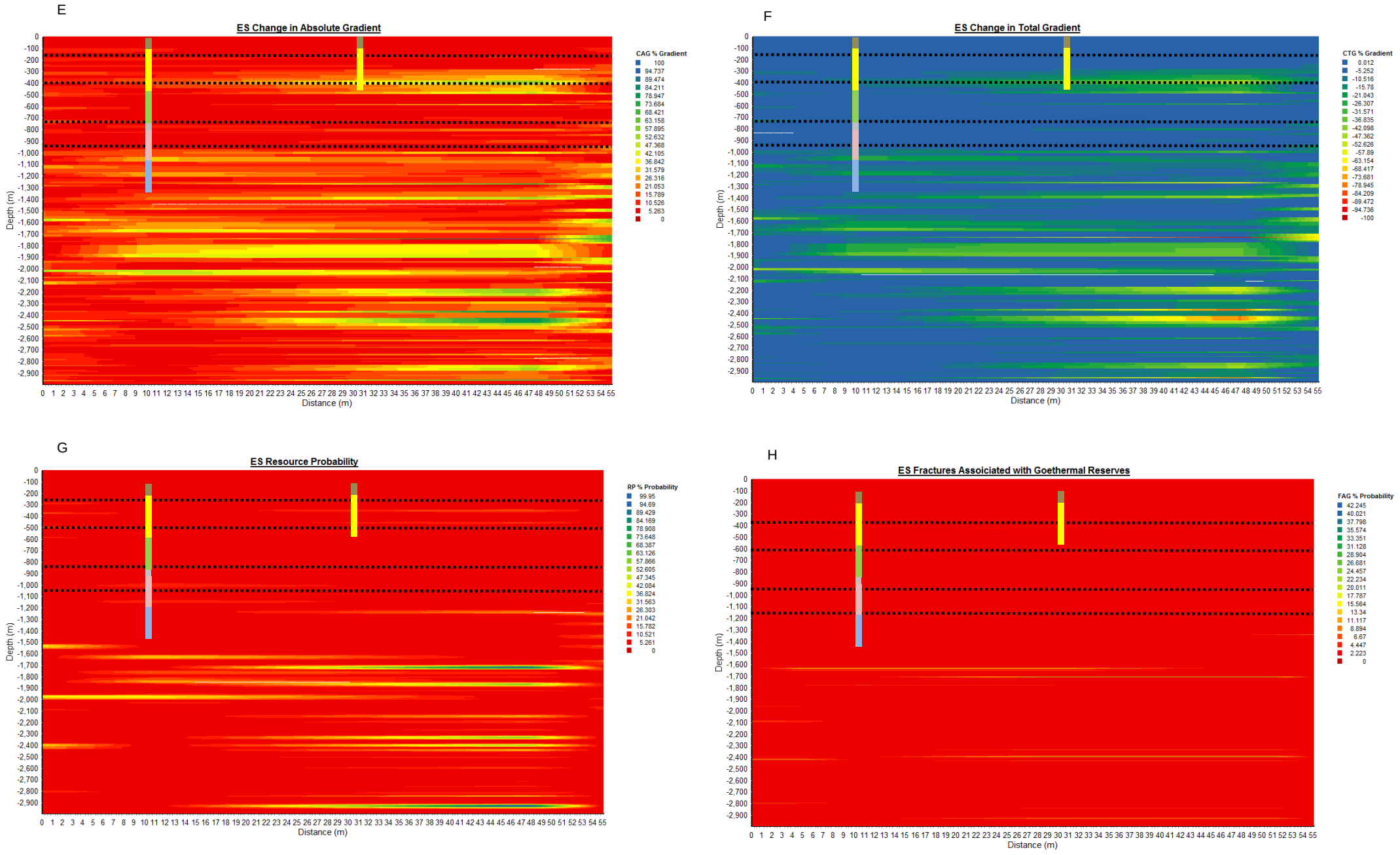

Figure 4 – Electro Seismic Data Analysis continued

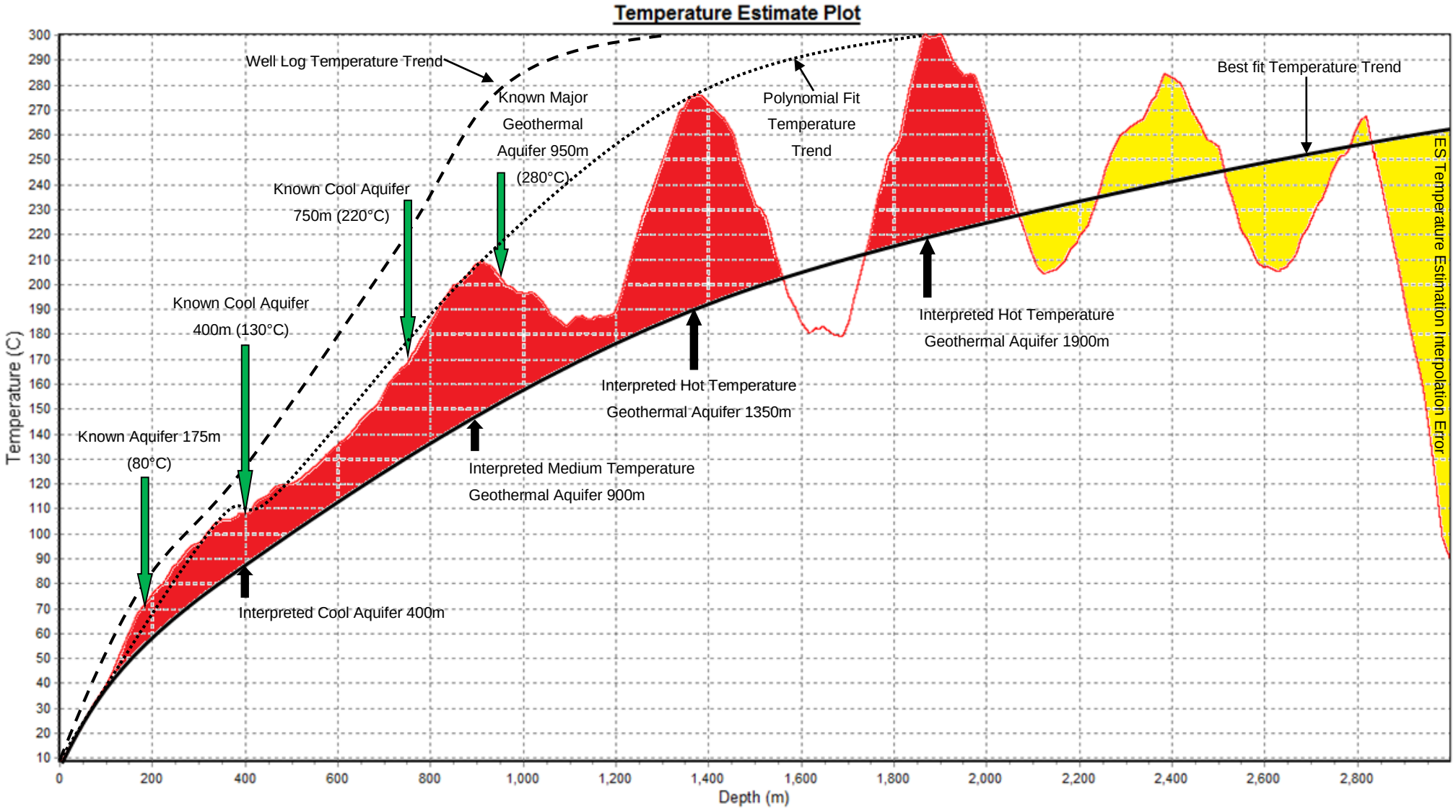

Figure 5 – Electro seismic Temperature Estimate Interpretation ***(Initial interpretation as presented to Contact Energy)***

This indicates change of geology or an interface between two geologies with large electrical property differences. This is supported by the well log data shown in Tables 4 and 5. The fracture tomography data, shown in Figure 4C, does not show any fracturing in the depth range of the aquifer, indicating that the aquifer does not have high secondary permeability. As such the aquifer have a low to medium flow rate. The resource probability data, shown in Figure 4G, shows that there is a high probability of geothermal resource at 950m depth. The aquifer at 175m is not clearly visible on the ES temperature estimation plot, shown in Figure 5. This may be due to the close temperature match between the best fit data and the actual aquifer temperature, thus indicating a very good temperature estimation but it does not help visually delineate the aquifer on Figure 5. This aquifer is of very low primary permeability as indicated by the hydraulic conductivity data. The aquifer is also visible in the ESCCT data, shown in Figure 4B, as a very week geothermal reserve. This could be attributed to the lower temperature of 80°C compared to the hotter aquifers under it. The aquifer is not represented in the ESCAGT and ESCTGT shown in figures 4E and F. The Resource probability data shown in Figure 4G indicates that the aquifer is not a potential geothermal resource. The aquifer does not appear to have any fracturing as such it is considered to be a low flow rate aquifer. The aquifer at 750m is not clearly visible on the ES temperature estimation plot, shown in Figure 5. This may be due to the close temperature match between the best fit data and the actual aquifer temperature, thus indicating a very good temperature estimation but it does not help visually delineate the aquifer on Figure 5. This aquifer is of very low primary permeability as indicated by the hydraulic conductivity data. The aquifer is also visible in the ESCCT data, shown in Figure 4B, as a very week geothermal reserve. The aquifer is represented in the ESCAGT and ESCTGT shown in figures 4E and F as a weak change of response gradient. This is interpreted as a geological formation change which is supported by the well log data in Tables 4 and 5. The Resource probability data shown in Figure 4G indicates that the aquifer is not a potential geothermal resource. The aquifer does appear to have fracturing as indicated on Figure 4C. This may explain why it has flow due to secondary permeability. There are three deeper aquifers at 1350m and 1900m depth. These aquifers will not be discussed as they have no supporting well log data. The aquifer summary is shown in Table 7.

Table 7 Site Comparative Hydrology

Known Aquifer Depths	ES Estimated Aquifer Depths
175m	Not clearly Visible
400m	400m
750m	Not Clearly Visible
950m	900m
Beneath Drill Depth	1350m
Beneath Drill Depth	1850m

6.2 Electro Seismic Temperature Estimation Interpretation

The ES temperature estimation tool was employed to determine the depth of aquifers under the site and whether the aquifers are considered cool or hot. This is done by including a best fit curve to the ES temperature estimation data. This best fit curve is the site temperature trend. Any temperature anomalies in the form of ES tempeature estimate deviations from this trend curve is interpreted as an aquifer. Normally negative deviations are interpreted as cool aquifers and postitive deviations are interpreted as hot aquifers. However, the actual temperature estimate may indicate a hot aquifer even on a negative deviation. Figure 5 also indicates the posistions and temperature estimates for all detected aquifers. Figure 5 shows interpreted cool aquifers as blue and hot aquifers as red. Using a best fit trend line gives a good indication on cool or hot aquifers, however it does not give the best indication of actual general site temperature trends. To find the best general formation temperature trend fit a polynomial fit on the peak ES temperature estimation peaks is done. This is indicated in Figure 5. A comparison between the polynomial fit and the actual temperatue trend, also shown in figure 5, shows the polynomial fit is a far better estimate of the site temperature trend. In general the temperature estimation is 30°C lower than the actual well log data, however this can be corrected by proper calibration of the temperature estimate. The ES temperature estimation model only applies to 2100m depth, after which the algorythm fails to produce reasonable results as indicated by the yellow section shown in figure 5.

7 Conclusions

This comparative study demonstrates that the electro seismic permeability tomography, ESCCT, ESFT, ESIT and ES temperature estimate geophysical methods show good correlation with the Test wells geological, lithological, temperature and hydrological well logs. Although

a great deal more study and testing is required to refine electro seismic methods and techniques, this study indicates that the electro seismic method can be used to effectively delineate and map geothermal resources, permeability, fracturing and geological interfaces. The ES temperature estimation method also shows potential at mapping hot rock formations for enhanced geothermal systems, however this method also needs to be tested further.

9 References

Frenkel, J. (1944) On the theory of seismic and seismoelectric phenomena in moist soil. Journal of Physics (Soviet). 230-241.

Pride, S. R. (1994) Governing equations for the coupled electromagnetics and acoustics of porous media. Physical Review B. 50, 15678–15696.

Blau, L. W. and Statham, L. (1936) Method and apparatus for seismic-electric prospecting. U.S Patent 2054067.

Haartsen, M. W., Dong, W. and Toksöz, M. N. (1998) Dynamic streaming currents from

seismic point sources in homogeneous poroelastic media. Geophysical Journal International. 132, 256-274.

Millar, J. W. A. and Clarke, R. H. (1997) Electrokinetic techniques for hydrogeological site investigations. Groundflow Ltd, Marlborough.

Du Preez, M. (2005) Accuracy of Electro-Seismic Techniques Applied to Groundwater Investigations in Karoo Formations. Unpublished Master Thesis: University of the Free State.

Du Preez, M and McKendry, J.R. (2010) Comparative Study of an Electro Seismic Investigation of the TH10 geothermal well located on the Tauhara Geothermal system near Taupo, NZ. Aquatronic Solutions Ltd, New Zealand.

Pride, S. R. and Morgan, F. D. (1991) Electrokinetic dissipation induced by seismic waves. Geophysics. 56 (7), 914–925.

Fitterman, D. V. (1978) Electrokinetic and magnetic anomalies associated with dilatant regions in a layered earth. Journal of Geophysical Research. 83 (B12), 5923–5928.